SAR and scan-time optimized 3D whole-brain double inversion recovery imaging at 7T

SAR and Scan-Time Optimized 3D Whole-Brain Double Inversion Recovery Imaging at 7T

Eberhard D. Pracht,[1]* Thorsten Feiweier,[2] Philipp Ehses,[3] Daniel Brenner,[1] Alard Roebroeck,[4] Bernd Weber,[5] and Tony Stöcker[1,6]

Purpose: The aim of this project was to implement an ultra-high field (UHF) optimized double inversion recovery (DIR) sequence for gray matter (GM) imaging, enabling whole brain coverage in short acquisition times (≈5 min, image resolution 1 mm^3).
Methods: A 3D variable flip angle DIR turbo spin echo (TSE) sequence was optimized for UHF application. We implemented an improved, fast, and specific absorption rate (SAR) efficient TSE imaging module, utilizing improved reordering. The DIR preparation was tailored to UHF application. Additionally, fat artifacts were minimized by employing water excitation instead of fat saturation.
Results: GM images, covering the whole brain, were acquired in 7 min scan time at 1 mm isotropic resolution. SAR issues were overcome by using a dedicated flip angle calculation considering SAR and SNR efficiency. Furthermore, UHF related artifacts were minimized.
Conclusion: The suggested sequence is suitable to generate GM images with whole-brain coverage at UHF. Due to the short total acquisition times and overall robustness, this approach can potentially enable DIR application in a routine setting and enhance lesion detection in neurological diseases.

Key words: DIR; EPG; UHF; SAR

INTRODUCTION

The double inversion recovery (DIR) sequence was first described by Redpath and Smith (1) to perform gray matter (GM) imaging in the human brain. The most common DIR application is lesion detection in multiple sclerosis (2–6). In contrast to fluid attenuated inversion recovery imaging (7) the DIR sequence not only minimizes partial volume effects from CSF signal but also from white matter. Despite the potential benefits, the DIR method has not been widely used for several reasons: After the initial magnetization preparation only approximately 10% of the equilibrium magnetization is left for imaging, reducing the remaining image SNR significantly (8). Furthermore, to selectively excite GM, long inversion times are needed. The DIR preparation time takes approximately 4 s, which leads to a low imaging sensitivity (which we defined as: $SNR/\sqrt{T_{AQ}}$). One potential solution to shorten scan time is the application of TSE imaging sequences with long echo trains. However, this induces blurring in the resulting images due to T_2 relaxation and increases the specific absorption rate (SAR). Taken together, the overall imaging sensitivity of DIR acquisitions is low. Thus, large volume coverage (i.e., whole brain imaging at high image resolution) is very time consuming, rendering the routine use of this method impractical.

Several optimizations to the DIR sequence were proposed over the last years to improve SNR and reduce scan time: To enable whole brain coverage, multi-slice and multi-slab approaches were proposed (9,10). However, only after the development of 3D non-selective variable flip angle (vFA)-TSE imaging (11,12), DIR imaging became feasible in a routine setting. This technique offers the possibility to eliminate most of the aforementioned problems. Compared to the standard TSE approach, vFA-TSE acquisitions produce less SAR and achieve higher image quality due to an improved point spread function (PSF) (12–14). In combination with improved reordering schemes (14,15) the total scan time can be reduced. To benefit from the increase in signal to noise ratio at ultra-high field (UHF), DIR imaging has been performed at 7T (16–18). However, despite the higher SNR, several drawbacks prevent the routine application of DIR at 7T: Longer tissue T_1 relaxation times reduce the overall scanning efficiency, and larger B_0 and B_1 inhomogeneities degrade image homogeneity and quality. Furthermore, the increase of RF power deposition with field strength and the prolonged longitudinal relaxation times cause lengthy repetition times. Another UHF related issue is the increase of the fat/water signal ratio with the field strength (16) as the T_1 of fat is less field strength dependent. Compared to 3T, the fat/water signal ratio of DIR acquisitions increases approximately by a factor of two at 7T. This leads to severe aliasing artifacts if parallel imaging is used. These artifacts are particularly pronounced in GM imaging due to the low signal contributions of GM compared to the fat signal. As shown by Madelin et al., a standard fat saturation is ineffective at 7T due to B_0 and B_1 inhomogeneities (16). The authors used a fat selective inversion instead and demonstrated that it is more efficient; however, at the expense of increased SAR.

[1]German Center for Neurodegenerative Diseases (DZNE), Bonn, Germany.
[2]Siemens Healthcare GmbH, Erlangen, Germany.
[3]Max Planck Institute for Biological Cybernetics, Tübingen, Germany.
[4]Department of Cognitive Neuroscience, Faculty of Psychology and Neuroscience, Maastricht, Maastricht University, The Netherlands.
[5]Department of Epileptology, University Hospital Bonn, Bonn, Germany.
[6]Department of Physics and Astronomy, University of Bonn, Bonn, Germany.
*Correspondence: Eberhard Pracht, Ph.D., Deutsches Zentrum fuer Neurodegenerative Erkrankungen e.V. (DZNE), Sigmund-Freud-Strasse 27, 53127 Bonn, Germany, E-mail: eberhard.pracht@dzne.de

Thorsten Feiweier is an employee of Siemens Healthcare. Thorsten Feiweier owns stocks of Siemens AG. Thorsten Feiweier holds patents filed by Siemens.

Received 27 March 2017; revised 28 July 2017; accepted 18 August 2017
DOI 10.1002/mrm.26913
Published online 14 September 2017 in Wiley Online Library (wileyonlinelibrary.com).

In this work, we present an optimized DIR imaging approach for UHF, based on a 3D vFA-TSE imaging sequence. We combined and optimized existing methods in order to reduce UHF related problems: To decrease SAR, improve the PSF and image quality we implemented an extended phase graph (EPG) optimized TSE imaging module (11,12). The excitation of each flip angle train is performed using a water excitation to decrease fat artifacts in the resulting images (19,20). Moreover, we utilize improved reordering schemes to minimize scan time and customize T_2 contrast in the acquired images (15). To mitigate image artifacts induced by B_0 and B_1 inhomogeneities, we optimized the DIR preparation module and replaced the standard inversion pulses with pulses tailored for UHF applications (21). Furthermore, we automated the inversion time calculation by integrating it into the signal calculation.

METHODS

The refinement of the DIR-sequence consists of the following three basic steps:

1. Implementation of an improved, fast and SAR efficient TSE imaging module
2. Utilization of improved reordering schemes
3. Optimization of the DIR preparation

TSE Imaging Module

For image acquisition, a customized 3D non-selective vFA-TSE module was implemented which acquires predefined signal shapes along the echo trains (Fig. 1). The calculation of the vFA trains is based on the EPG algorithm (22). The (normalized) target signal shape, $f(n)$, is chosen to follow an exponential decay (decay rate λ) with an initial plateau. Preceding the plateau five dummy echoes ($N_d = 5$) are acquired, prepending an exponential signal decay before the plateau (decay rate λ_d):

$$f(n) = \begin{cases} e^{-(n-1)\pi\lambda_d/N_d}, & 0 < n \le N_d \\ e^{-(N_d-1)\pi\lambda_d/N_d}, & N_d < n \le N_c \\ e^{-(N_d-1)\pi\lambda_d/N_d} e^{-(n-N_c)\pi\lambda/(N_p-N_c)} & N_c < n \le N_p \end{cases} \quad [1]$$

where N_p denotes the number of refocusing pulses per echo train and N_c the center echo number. This shape offers a good compromise between image SNR and image blurring, as it creates a narrow PSF (11). The five initial refocusing pulses are used to prepare the magnetization close to the static pseudo steady state (23) in order to reach higher initial signal amplitude. Figure 2 depicts target signal shapes and the corresponding PSFs for different decay rates (the first exponential decay is set to zero in the Figure for clarity).

The flip angles of the refocusing pulses are optimized iteratively to produce a signal response with the predefined target shape along the echo train. The first refocusing angle is given as an input parameter in the EPG simulation. The corresponding EPG echo amplitude ($F_{-1}(1)$, following the notation in (12)) is calculated and then the next flip angle is determined by finding the root of

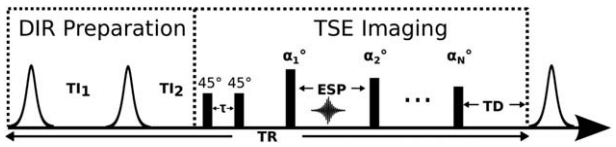

FIG. 1. Schematic timing diagram of the optimized DIR-sequence. After the DIR preparation a binomial water excitation pulse is applied for fat suppression. The excitation pulses are separated by τ such that the fat component precesses 180° (resulting in a net flip angle of zero degrees for the fat component). The echo train is acquired using the shortest possible echo spacing (ESP) to avoid signal loss due to T_2 decay. The refocusing angles are calculated to generate echoes with predefined signal amplitudes for gray matter. After a relaxation delay TD the next inversion pulse of the following TR is played out.

$$\Gamma(\alpha_n) \equiv |F_{-1}(n) - F_{-1}(1)f(n)|, \;\; n = 2, \ldots, N_p \quad [2]$$

where $F_{-1}(n)$ denotes the amplitude of the nth echo. If the difference between the calculated echo amplitude, $F_{-1}(n+1)$, and the target signal, $F_{-1}(1)f(n)$, is larger than a given tolerance the flip angle calculation is aborted and started again using a smaller first refocusing angle. This approach is similar to a previously published and established method (24) and is closely related to Mugler's signal shaping algorithm (25). In contrast to Mugler's isochromat averaging method we utilize the EPG algorithm, because it is less computationally demanding and easier to implement. This procedure can be considered as a brute force version of Hennig's recursive 1-ahead algorithm (12) and yields similar flip angle trains. The maximum possible signal level for a given target shape is obtained by applying a binary search to the first flip angle (searching in the interval between 0° and 180°). The iteratively calculated flip angle train which applies the maximum possible first flip angle yields the maximum SNR for the given target shape.

The computation of the inversion times TI_1/TI_2 is also integrated into the EPG based flip angle calculation algorithm. For simplicity, instantaneous inversion is assumed and all transverse EPG states are neglected during the DIR preparation interval ($T_2 \ll TI_{1,2}$) and only the Z_0-state (unmodulated longitudinal magnetization (12)) is considered, because longitudinal magnetization regrowth (i.e., T_1 recovery) occurs only in this state (recovering magnetization is necessarily unmodulated).

The repetition time TR of the DIR sequence is defined as the sum of the inversion preparation times ($TI_1 + TI_2$), and the acquisition time for one TSE echo train (including a relaxation delay TD at the end of the echo train), see Figure 1. Solving the Bloch equation for the z-component of the magnetization yields:

$$M_z(TI_1 + TI_2) = M_0 + E_2[\varepsilon^2 M_z(TR)E_1 + \varepsilon M_0 E_1 - (1+\varepsilon)M_0] \quad [3]$$

using

$$E_{1,2} = e^{-TI_{1,2}/T_1} \quad [4]$$

where M_0 denotes the equilibrium magnetization, T_1 reflects the longitudinal relaxation time, and ε denotes

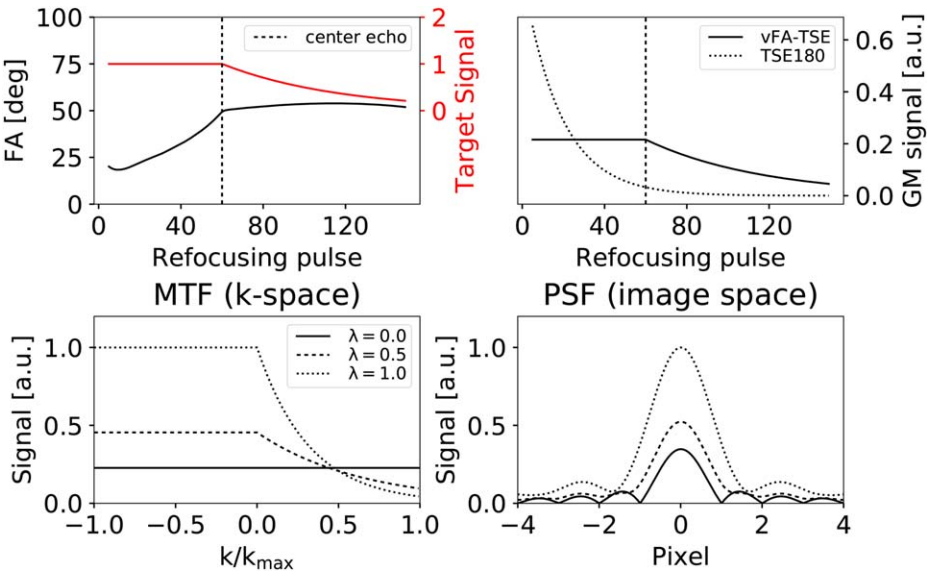

FIG. 2. Signal shaping simulations. Top left: Calculated flip angle train for gray matter (target signal depicted in red). Top right: Resulting gray matter signal (compared to the theoretical signal evolution of a TSE sequence employing 180° pulses, dashed). The initial exponential decay into the plateau (five dummy pulses) is omitted. Bottom: Signal evolution for different target signal shapes in k-space and image space. Flatter signal envelopes (smaller decay rates λ) of the modulation transfer function (MTF) in k-space yield a narrower point spread function (PSF). This results in less blurring, but lower SNR in image space.

the inversion efficiency of the inversion pulses. M_z(TR) equals the Z_0 state of the EPG simulation, which describes the unmodulated longitudinal magnetization state of the vFA-TSE imaging module after TR. For $\varepsilon = 1$ and $TR \gg T_1$ the solution turns into Equation [1] of the Redpath publication (1).

For GM imaging, inversion times have to be adjusted to suppress CSF and white matter signal simultaneously. Hence, the longitudinal magnetization components of the undesired tissue components (gray and white matter) have to equal zero after the DIR preparation ($M_z(TI_1 + TI_2) \stackrel{!}{=} 0$), leading to:

$$E_2 = M_0/((1+\varepsilon)M_0 - \varepsilon^2 M_z(TR)E_1 - \varepsilon M_0 E_1) \quad [5]$$

Using Equation [4] it follows:

$$TI_2 = -T_1 \ln(E_2) \quad [6]$$
$$= -T_1 \ln(M_0/[(1+\varepsilon)M_0 - \varepsilon^2 M_z(TR)E_1 - \varepsilon M_0 E_1] \quad [7]$$

The desired inversion times TI_1 and TI_2 are derived via numerical optimization by finding the root of:

$$\Gamma(TI_1) = TI_2^{WM} - TI_2^{CSF} \quad [8]$$

As the magnetization is not fully recovered after one TR, M_z(TR) evolves and changes the following TRs. For that reason dummy TRs were included until M_z(TR) reached a steady state (usually three dummy repetitions were sufficient).

An alternative (graphical) approach to solve this problem is given in the original publication by Redpath and Smith (1).

To be able to reduce SAR independent of the sequence timing and contrast, a mechanism was implemented which allows to recalculate the echo train with reduced flip angle amplitudes, while simultaneously preserving the shape of the target signal. The first refocusing flip angle of the echo train (which was determined by the binary search) is reduced by a factor R ($\alpha_{1,red} = R \cdot \alpha_1$) and the remaining refocusing pulses are recalculated for the prescribed target shape. The rationale behind the applied procedure is to keep more magnetization longitudinal along the echo train, to store it there ($T_1 \gg T_2$), and prevent further decay as time passes along the echo train. Note that recalculation with $R<1$ results in a new flip angle train which still exactly matches the shape of the prescribed target signal but with a lower signal level. This is superior to decreasing the transmitter reference voltage, which would change the target signal shape and therefore the PSF. The relative SAR applied during one SAR optimized vFA-TSE train ($R<1$) compared to the SNR optimized echo train ($R = 1$) was calculated similar to (26):

$$SAR_{rel} = \frac{100\%}{N_p} \cdot \sum_{i=1}^{N_p} \left(\frac{\alpha_i^{R<1}}{\alpha_i^{R=1}} \right)^2 \quad [9]$$

where N_p denotes the number of refocusing pulses. Due to the quadratic relationship of SAR with flip angle, SAR drops significantly when reducing the refocusing angles. The SAR percentage decrease is larger than the SNR loss due to the aforementioned longitudinal storage of magnetization. In addition, to keep SAR as low as possible, a water excitation was implemented in order to eliminate fat signal contributions (see Fig. 1). The implemented method is based on 1–1 binomial pulses and uses a $45° - \tau - 45°$ composite pulse such that the fat component precesses 180° during the interval between the pulses (19). The sequence timing is not affected for the binomial excitation, as the minimum echo spacing is limited by the readout interval. The water excitation method was compared to the spectrally selective fat suppression method proposed by Madelin et al. (16).

DIR Preparation

Standard hypersecant (HS1) inversion pulses are less homogeneous at UHF due to B_0 and B_1 variations over the FOV. Hence, parts of the longitudinal magnetization in the brain are not properly inverted. To overcome this issue, HS6 pulses were implemented to improve inversion

homogeneity (27). These pulses are designed to produce high inversion homogeneity over a specified bandwidth using a reduced peak power. Our implementation is based on the work of Tesiram et al. (21), using the following pulse parameters: 10.24 ms duration, 2 kHz bandwidth, ± 1.2 kHz frequency sweep, 0.3 kHz (≈ 7 μT) peak amplitude, 99% desired inversion efficiency, and 10% maximum inversion error. To fine-tune the inversion homogeneity (especially in low B_1 brain regions) the peak power of the HS6 pulses was increased manually until satisfying inversion homogeneity over the whole brain was achieved. If SAR limitations were violated, the SAR reduction technique mentioned earlier was applied until SAR restrictions were met (by reducing the first refocussing flip angle manually and recalculating the echo train).

In Vivo Experiments

All experiments were acquired on a 7T whole-body research system (Siemens Healthcare GmbH, Erlangen, Germany; Magnet: Agilent, Oxford, UK) using a head array coil (32Rx/1Tx, Nova Medical, Wilmington, MA). The MR scanner is equipped with a gradient system allowing maximum gradient amplitude of 70 mT/m and a maximum slew rate of 200 T/m/s. Imaging was performed in five healthy volunteers. The study protocol was approved by the local ethics committee, and subjects gave informed consent prior to undergoing MR examination. At the beginning of each imaging session, a shim over the whole head up to the 3rd order was applied to homogenize the main magnetic field. Afterwards, combined B_0 and B_1-mapping was performed using 3DREAM (28) a three dimensional variant of the DREAM sequence (29). Subsequently, GM imaging was performed. To speed-up the DIR acquisition, an improved linear reordering scheme was implemented (15). It allows to omit the corners of k-space (k_y–k_z plane), which is also known as elliptical scanning (30). In contrast to standard linear view ordering the echo train length is not restricted to the number of partitions. Applying both, elliptical scanning and partial Fourier acquisitions simultaneously, the total scan time can be reduced by approximately 20%. If additionally parallel imaging is employed (acceleration factor $R_{PI} = 2 \times 2$) the total acquisition time of the imaging module can be accelerated by a factor of approximately eight compared to a non-accelerated acquisition ($R_{PI} = 1$) employing standard linear reordering. Imaging parameters for all 7T acquisitions were: Number of refocusing pulses $N_p = 150$, repetition time TR = 11,000 ms (TR and N_p were adjusted to maximize the imaging sensitivity (which we defined as: $SNR/\sqrt{T_{AQ}}$), 1 × 1 × 1 mm^3 resolution, matrix size 256 × 248 × 160 (whole brain coverage), $TI_1/TI_2 = 3257/627$ ms, 2D-GRAPPA with a reduction factor of $R_{PI} = 4$ (2 × 2). The T_1 brain tissue relaxation times used for the TI calculation at 7T were set to: GM: $T_1 = 1780$ ms, white matter: $T_1 = 1230$ ms, and CSF: $T_1 = 4300$ ms (31). For the EPG signal shape computation, the GM tissue T_2 relaxation was set to $T_2 = 55$ ms (32). The duration for the non-selective refocusing and inversion pulses was 700 μs and 10.24 ms, respectively. Total scan time was 6:58 min.

To assess the inversion efficiency of the HS6 pulses an inversion recovery turbo-flash series ($TI = 10$, 300, 600, 900, 1200, 1800, 2400, 3000, 4000, 5000 ms) was acquired in one volunteer (the inversion sensitivity is subject independent). The signal time series was fitted to the following equation (using non-linear least squares minimization):

$$S(TI) = S_0(1 - (1 + \varepsilon)e^{-\frac{TI}{T_1}}) \quad [10]$$

where ε denotes the inversion efficiency and S_0 describes the signal intensity without inversion. For the flip angle of the inversion pulses (needed for the EPG signal calculation) follows:

$$\alpha_{INV} = \frac{\arccos(-\varepsilon)}{\pi} \cdot 180^{\circ} \quad [11]$$

For all acquisitions, the transmitter voltage was adjusted to cortical GM (the calculation was based on the acquired B_1 maps). GM was chosen rather than the global mean across the brain in order to optimize the flip angle train (and therefore the PSF) to this region. The cortex is highly folded and thus benefits most from a narrow PSF.

To investigate the SAR dependency on the flip angle reduction factor, GM images with $R = 1$, 0.95, and 0.9 were acquired. The remainders of the sequence parameters were kept identical. The scans comparing the different fat suppression techniques (no fat suppression vs. fat selective inversion vs. water excitation) were acquired with a flip angle reduction factor of 0.9, to stay within SAR limits for the fat selective inversion technique (the method inducing the highest SAR). The comparison of the HS1 and HS6 inversion preparation was performed using the same sequence parameters. Additionally, for comparison of the field strength dependence (inversion efficiency and scan sensitivity) a scan at 3T (MAGNETOM Skyra, Siemens), 32 channel head array coil) was acquired for one volunteer using identical sequence parameters to the 7T acquisitions, but with tissue T_1 relaxation times matched to 3T: GM: $T_1 = 1300$ ms, White matter: $T_1 = 890$ ms, and CSF: $T_1 = 4300$ ms (31). Additionally, the repetition time was changed to TR = 10000 ms and the number of RF pulses to $N_p = 235$ (in order to maximize the imaging sensitivity). The T_2 in the signal shaping algorithm was set to $T_2 = 110$ ms (33). The change in relaxation times resulted in lower inversion times: $TI_1/TI_2 = 3073/588$ ms. The GM SNR calculations were performed using the pseudo multiple replica method described by Robson et al. (34).

RESULTS

Using the average T_1 brain tissue relaxation times at 7T ($T_{1WM}/T_{1GM} \approx 1200/1800$ ms) for the inversion time calculation of the DIR preparation did not suppress white matter and CSF signal in the in vivo scans sufficiently. Inclusion of the measured HS6 inversion efficiencies ($\varepsilon_{WM} \approx 0.76$, $\varepsilon_{GM} \approx 0.9$, $\varepsilon_{CSF} \approx 0.99$) into the signal model solved this issue and yielded corrected inversion times ($TI_1/TI_2 = 3257/627$ ms). A representative axial slice of a

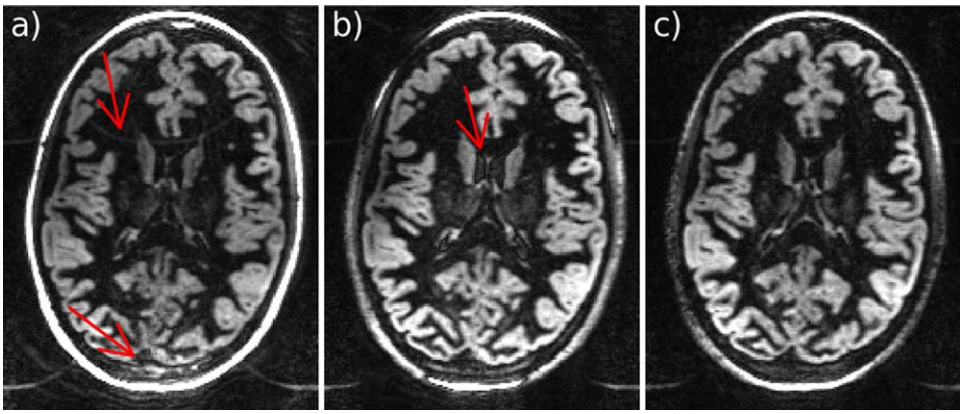

FIG. 3. Gray matter images of a healthy subject at 7T: **a**: No fat suppression applied, severe aliasing fat artifacts compromise image quality (red arrows). **b**: Fat suppression based on frequency selective inversion (20) almost completely removes these artifacts, but signal suppression is slightly affected (red arrow). **c**: The application of a SAR efficient water excitation results in a similar degree of fat suppression.

DIR GM acquisitions at 7T (using the EPG optimized flip angle and inversion time calculation) are shown in Figure 3c. Signal from white matter and CSF was completely suppressed. No significant image blurring, induced by T_2 relaxation during the echo train acquisition was observed. For the 3T measurement the implemented inversion time calculation worked as expected without compensation for the inversion efficiency ($\varepsilon_{WM} = \varepsilon_{GM} = \varepsilon_{CSF} = 1$).

Fat Suppression

Aliasing artifacts originating from fat (Fig. 3, left) severely compromise image quality at 7T. Application of fat suppression techniques significantly reduced these artifacts (while the GM signal remains unaffected, Fig. 3, middle and right). However, the SAR increased significantly for the chemical shift based inversion method (16), because of the application of an additional inversion pulse per repetition. Furthermore, signal suppression was slightly affected. Contrarily, for the water excitation based acquisition (Fig. 3, right) the total SAR per acquisition slightly decreased (due to the separation of the 90° pulse into two 45° pulses). The fat suppression of the water excitation efficiency was comparable to the inversion method.

SAR Reduction

When the SAR limits for a given parameter set were exceeded, the flip angle trains were recalculated using the described SAR reduction technique. The top row of Figure 4 shows the simulated flip angle trains and signal envelopes with (flip angle reduction $R = 0.9$) and without ($R = 1.0$) the SAR reduction technique. The remainders of the imaging parameters were kept identical. The application of this technique effectively decreased the total SAR down to 70%, while the image SNR remained at approximately 90% of the initial signal level. The bottom right plot of Figure 4 depicts the signal amplitude and SAR change for different reduction factors. The imaging results (see Fig. 5) confirmed the theoretically predicted ones: SAR was reduced significantly, while the image SNR decreased only by approximately 10% (the depicted SAR

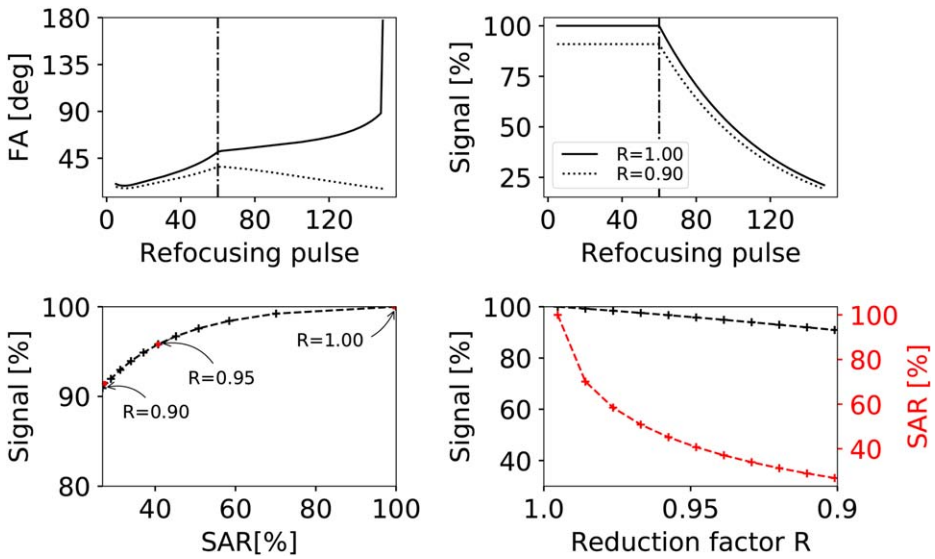

FIG. 4. Example SAR simulation results. Top: Flip angle calculation (left) and resulting signal evolution (right) with and without applied SAR reduction technique. Bottom: Signal intensity and relative SAR of an refocusing train (inversion pulses not included) for different flip angle reduction factors (calculated using equation 9). The SAR decreases significantly with the reduction factor, while the image SNR only drops by 10%.

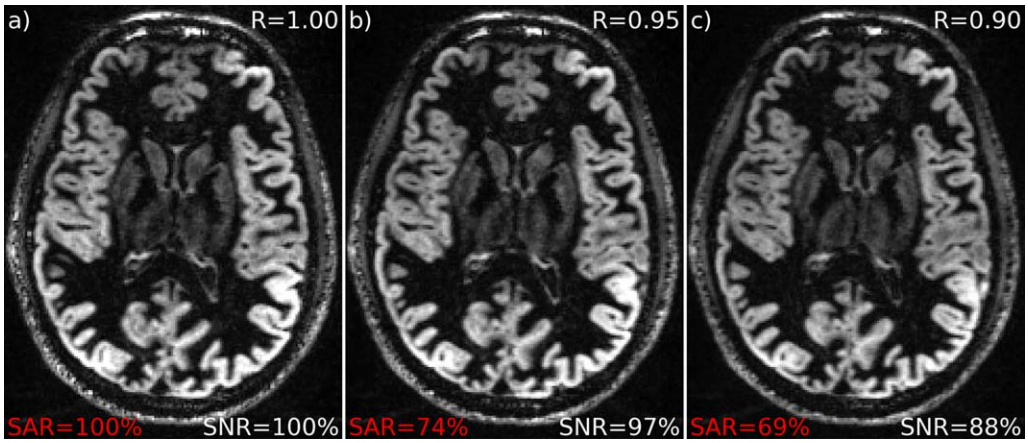

FIG. 5. Application of the SAR reduction technique. Left: DIR acquisition without flip angle amplitude reduction. Middle, right: Measurements with SAR-reduction ($R = 0.95$ and $R = 0.90$). The global SAR (calculated by the scanner) drops down to 69% of the original value, while the SNR remains at 88% (for a reduction factor of $R = 0.90$).

values in Fig. 5 are given as displayed by the scanner). Image blurring and contrast remained the same with and without the SAR reduction technique, as the same signal shape and sequence parameters form the basis for all flip angle calculations.

Magnetization Preparation

Figure 6 shows the impact of B_0 and B_1 inhomogeneities on GM acquisitions at UHF. Compared to 3T acquisitions the image intensity was more inhomogeneous, due to imperfect magnetization inversion. If standard hypersecant (HS1) inversion pulses were used, severe signal dropouts occurred in the GM images at 7T. Furthermore, due to the use of a local head transmit coil, loss of transmitter sensitivity in caudal brain regions occurred (at the level of the cerebellum). Application of the HS6 pulses reduced these signal dropouts in GM and the image intensity appeared more homogeneous over the whole imaging volume. Some of these remaining dropouts could potentially

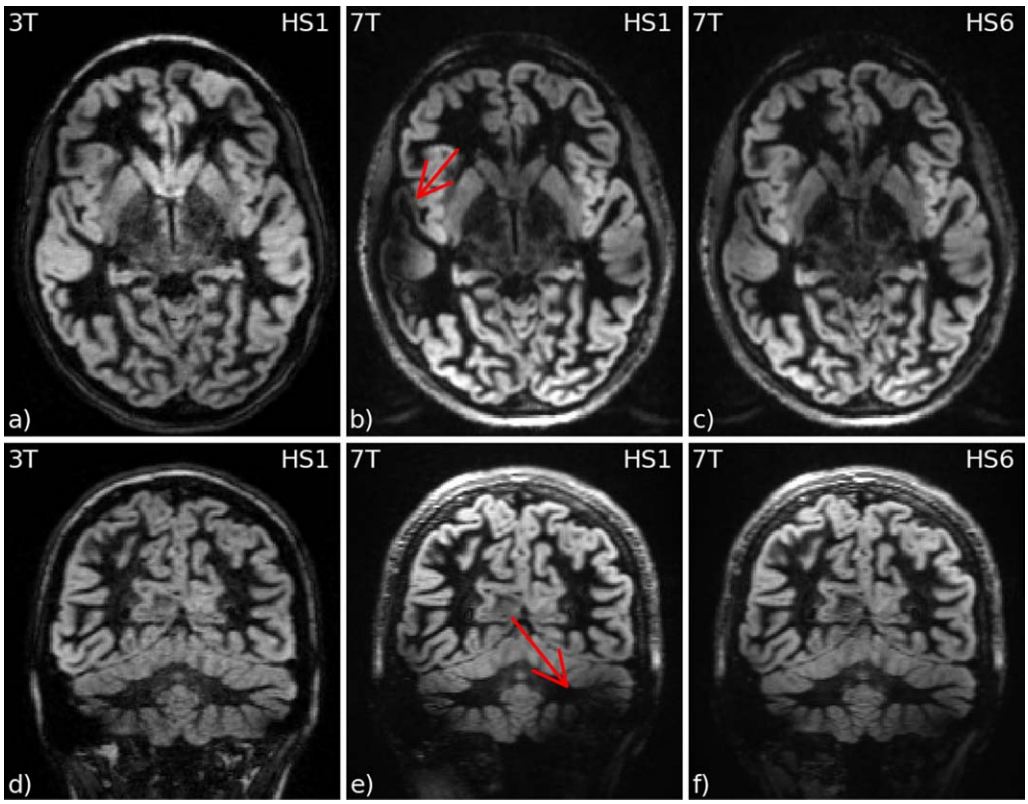

FIG. 6. Comparison of standard and optimized inversion preparation at 7T. At 3T the standard inversion is sufficient (left) to achieve complete inversion over the whole brain volume. Whereas at 7T signal drop outs occur when standard HS1 pulses are applied (middle, red arrows). The substitution to HS6 pulses increased the inversion efficiency and reduced the signal dropouts over the imaging volume (right).

be reduced by further increasing the peak power of the HS6 pulses. The average GM sensitivity after applying the whole optimization procedure was by a factor of approximately 1.5 higher at 7T. Theoretically, the sensitivity increases by a factor of approximately 1.7.

DISCUSSION

This work demonstrates that it is possible to obtain whole brain GM images at 7T with an isotropic resolution of 1 mm in scan times below seven minutes. Furthermore, we show that the image contrast of the proposed method is highly customizable. The DIR sequence remains sensitive to high-field specific issues—prolonged tissue T_1 relaxation, B_0 and B_1 inhomogeneities, SAR limitations and a dominant fat signal—which were all accounted for with appropriate sequence modifications.

Traditionally, the major limitations for DIR imaging at UHF are SAR constraints which prolong the acquisitions beyond clinically acceptable times. To solve this issue, we implemented repeats in the flip angle computation which reduces refocusing angles when SAR restrictions for a given parameter set are not met. Recalculating the flip angle train, while simultaneously keeping all other imaging parameters identical, allows one to significantly reduce SAR and maintain the image contrast with only 10% SNR loss. Thus, shorter repetition times can be applied without violating SAR constraints. An alternative approach to decrease SAR would be to increase the duration of the refocusing pulses. However, prolonging the pulse duration would lead to an increase in the inter pulse delay (which would reduce the imaging sensitivity) and decrease the pulse bandwidth.

Due to the short TR, full magnetization relaxation is not achieved at the end of the repetition time, resulting in a TR dependent longitudinal magnetization before each DIR preparation. To optimize and correct the signal suppression for the unwanted tissue types for short repetition times ($TR < 5\ T_1$), we integrated the *TI* calculation of the DIR preparation into the flip angle simulation.

Because of large B_0 and B_1 inhomogeneities at UHF adiabatic hypersecant inversion pulses (27) are less efficient and the magnetization is not homogeneously inverted over the imaging volume. The spatially modulated inversion efficiency gives rise to spatially modulated signal attenuation and dropouts over the FOV. This issue was already addressed in the past by several research groups (27). They proposed various inversion pulse designs customized to UHF imaging. We chose HSn pulses, as they are easy to implement and achieve sufficient inversion efficiency for the present purpose. For the given work we found HS6 pulses to be a very good compromise between off-resonance performance, peak power and time averaged power requirements. Doubling the peak power maximized the inversion homogeneity in the cerebellum (low B_1 region). In this case, the theoretical inversion efficiency of the HS6 pulses remains still at 99% due to the doubled peak power (assuming 50% of the maximum B_1 in the cerebellum). Thus, the limited ability to perform a homogeneous inversion in the cerebellum is caused by the rapid coil sensitivity drop in these areas. Hence, the inversion is primarily limited by the capped available peak amplitude of the amplifier (but also by SAR).

However, assuming complete inversion did not yield the expected results of perfect signal suppression. Significant white matter and CSF signal remained in the GM images. An additional T_1 quantification approach, based on an inversion recovery turbo-flash sequence showed that reduced inversion efficiency is the reason for this discrepancy. Longitudinal white matter ($\varepsilon \approx 0.76$) and GM ($\varepsilon \approx 0.9$) magnetization are not properly inverted at 7T due to this reduced inversion efficiency. Inclusion of the inversion efficiencies into the signal calculation model reduced the calculated inversion times and solved this issue. This effect is present in hypersecant (HS1), as well as HSn inversions ($n>1$) at 7T but not found at 3T. Norris et al. (35) investigated this phenomenon and found a T_2 dependence of the inversion efficiency. However, an inversion efficiency of 0.76 in white matter would need a T_2 of approximately 10 ms according to these simulations. Considering this, an additional mechanism has to further decrease the inversion efficiency. The underlying additional mechanism causing the reduced inversion efficiency is related to magnetization transfer, which was already observed and described by van Gelderen et al. (36). Magnetization transfer results in a clear deviation from single exponential relaxation at short TI. Hence, the accelerated recovery at short TI leads to an apparent inversion efficiency with $\varepsilon < 1$. The effect is field strength and inversion pulse type dependent and more prominent in white matter (due to high myelin content). An advantage of the apparent inversion efficiency is a concomitant shortening of the required inversion times, which is reducing the scan time additionally.

To further decrease scan time, we implemented improved reordering schemes (14). By applying elliptical scanning, parallel imaging, and the aforementioned SAR reduction technique, it is possible to reach clinically acceptable scan times. However, if parallel imaging is used to shorten the scan time, aliasing fat artifacts contaminate the images and degrade image quality. This effect was already investigated by Madelin et al. (16). They showed that a standard fat saturation is not sufficient at 7T and used a fat selective inversion instead. The major drawback of this solution is the large increase in SAR due to an additional inversion pulse per TR. Hence, we chose a water excitation instead to suppress the intense fat signal. By splitting the 90° excitation pulse into two 45° pulses, the SAR is even slightly decreased (due to the reduced B_1 peak power). The resulting fat suppression level is comparable to the fat selective inversion, removing the fat artifacts completely. Even better fat suppression could be achieved using longer spectral selection pulses (1-2-1 or 1-3-3-1 pulses). However, this would lead to an increase in echo spacing and reduce imaging sensitivity. It is important to note that the shimming procedure has to be applied over the whole head to obtain homogeneous fat suppression. If only the brain volume is shimmed, an incomplete suppression of the fat signal originating in the skull occurs as a consequence (as the water excitation is sensitive to off-resonances).

For the acquired sequence protocol a theoretical gain in SNR for GM at 7T of approximately 1.7 would be expected (calculated using the flip angle simulation routine, considering the shortened T_2 at 7T, and assuming a linear increase in M_0 from 3T to 7T). The average GM sensitivity gain at 7T of 1.5 was close to the theoretically predicted one. The slightly decreased sensitivity gain and the remaining signal intensity variations over the FOV are most likely induced by deviating flip angles (based on the spatially varying B_1 field) in the TSE echo trains. Therefore, it still remains an open question if DIR based lesion detection at 7T has equal sensitivity as compared to 3T. Regions with homogeneous B_1 and B_0 in 7T DIR images should deliver a better, or at least the same delineation due to the comparable SNR and sensitivity at 7T. However, even if all the improvements are included, the 7T images still lack homogeneity compared to lower field strength. For instance, the non-uniform B_1 field results in reduced signal intensity in the temporal lobes, and the theoretically predicted SNR gain for 7T (vs. 3T) is not achieved. The aforementioned intensity modulations over the imaging volume reduce contrast and hamper the detection of pathologies and lesions (18). Moreover, the sensitivity of the DIR method is still low compared to other structural MR imaging methods. Visser et al. developed a modified DIR preparation module, which combines the standard DIR preparation with a T_2 preparation module (MP-DIR preparation, (17)). This module reduces T_1 weighting during the magnetization preparation period (leading to shorter inversion times) and yields enhanced GM signal intensity. This approach seems promising, as the higher signal intensity combined with the shorter inversion times lead to an increased sensitivity. However, SAR restrictions force to prolong the total acquisition time, reducing or even removing the sensitivity gain.

Possible future improvements include the utilization of an adiabatic excitation pulse that could increase SNR and further reduce signal dropouts caused by B_1 inhomogeneities at the expense of SAR. A more homogeneous excitation/refocusing could be obtained by exploiting multi-channel transmit techniques such as kT-Points (37) or by the spatially resolved EPG (38). To accelerate imaging further compressed sensing techniques (39) could additionally be exploited (40). Future work will also be directed to assess the potential in a clinical research setting.

CONCLUSION

We show that high resolution (1 mm^3), 3D whole brain DIR imaging in short scan times ($\approx$ 7 min) is possible at 7T. We introduced several improvements to the DIR technique, such as an EPG optimized TSE imaging module, an efficient fat suppression technique, and an optimized inversion preparation. Compared to a standard DIR-TSE sequence (employing 180° refocusing pulses, HS1 inversion, standard linear reordering) these modifications reduce SAR significantly, decrease image blurring, and increase overall image quality. Furthermore, we show that a large scan time reduction is possible while still maintaining sufficient SNR.

ACKNOWLEDGMENTS

The authors would like to thank Scannexxus (Maastricht, Netherlands) for providing the necessary infrastructure to acquire the initial 7T DIR images.

REFERENCES

1. Redpath TW, Smith FW. Imaging gray brain matter with a double-inversion pulse sequence to suppress CSF and white matter signals. Magn Reson Mater Phys Biol Med 1994;2:451–455.
2. Geurts JJG, Pouwels PJW, Uitdehaag BMJ, Polman CH, Barkhof F, Castelijns JA. Intracortical lesions in multiple sclerosis: improved detection with 3D double inversion-recovery MR imaging. Radiology 2005;236:254–260.
3. Wattjes MP, Lutterbey GG, Gieseke J, Träber F, Klotz L, Schmidt S, Schild HH. Double inversion recovery brain imaging at 3T: diagnostic value in the detection of multiple sclerosis lesions. Am J Neuroradiol 2007;28:54–59.
4. Nelson F, Poonawalla AH, Hou P, Huang F, Wolinsky JS, Narayana PA. Improved identification of intracortical lesions in multiple sclerosis with phase-sensitive inversion recovery in combination with fast double inversion recovery MR imaging. Am J Neuroradiol 2007; 28:1645–1649.
5. Calabrese M, De Stefano N, Atzori M, et al. Detection of cortical inflammatory lesions by double inversion recovery magnetic resonance imaging in patients with multiple sclerosis. Arch Neurol 2007; 64:1416–1422.
6. Tallantyre EC, Morgan PS, Dixon JE, Al-Radaideh A, Brookes MJ, Morris PG, Evangelou N. 3 Tesla and 7 Tesla MRI of Multiple Sclerosis Cortical Lesions. J Magn Reson Imaging 2010;32:971–977.
7. De Coene B, Hajnal JV, Gatehouse P, Longmore DB, White SJ, Oatridge A, Pennock JM, Young IR, Bydder GM. MR of the brain using fluid-attenuated inversion recovery (FLAIR) pulse sequences. Am. J. Neuroradiol 1992;13:1555–1564.
8. Pracht ED, Feiweier T, Ehses P, Brenner D, Weber B, Stöcker T. SAR and scan-time optimized 3d whole-brain double inversion recovery (DIR) Imaging. In Proceedings of the 21st Annual Meeting of ISMRM, Salt Lake City, Utah, USA, 2013. Abstract 0249.
9. Bedell BJ, Narayana PA. Implementation and evaluation of a new pulse sequence for rapid acquisition of double inversion recovery images for simultaneous suppression of white matter and CSF. J Magn Reson Imaging 1998;8:544–547.
10. Boulby P, Symms MR, Barker GJ. Optimized interleaved whole-brain 3D double inversion recovery (DIR) sequence for imaging the neocortex. Magn Reson Med 2004;51:1181–1186.
11. Mugler JP. Optimized three-dimensional fast-spin-echo MRI. J Magn Reson Imaging 2014;39:745–767.
12. Hennig J, Weigel M, Scheffler K. Calculation of flip angles for echo trains with predefined amplitudes with the extended phase graph (EPG)-algorithm: principles and applications to hyperecho and TRAPS sequences. Magn Reson Med 2004;51:68–80.
13. Pouwels PJW, Kuijer JP, Mugler JP, Guttmann CRG, Barkhof F. Human gray matter: feasibility of single-slab 3D double inversion-recovery high-spatial-resolution MR imaging. Radiology 2006;241: 873–879.
14. Busse RF, Brau ACS, Vu A, Michelich CR, Bayram E, Kijowski R, Reeder SB, Rowley HA. Effects of refocusing flip angle modulation and view ordering in 3D fast spin echo. Magn Reson Med 2008;60:640–649.
15. Feiweier T. Magnetic resonance imaging data acquisition sequence and apparatus. US Patent 7728588B2 2010.
16. Madelin G, Oesingmann N, Inglese M. Double inversion recovery MRI with fat suppression at 7 Tesla: initial experience. J Neuroimaging 2010;20:87–92.
17. Visser F, Zwanenburg J, de Graaf W, Castelijns JA, Luitjen P. 3D magnetization prepared double inversion recovery (3D MP-DIR) at 7 Tesla. In Proceedings of he 18th Annual Meeting of ISMRM, Stockholm, Sweden, 2010. Abstract 2068.
18. de Graaf WL, Zwanenburg JJM, Visser F, Wattjes MP, Pouwels PJW, Geurts JJG, Polman CH, Barkhof F, Luijten PR, Castelijns JA. Lesion detection at seven Tesla in multiple sclerosis using magnetisation prepared 3D-FLAIR and 3D-DIR. Eur Radiol 2012;22:221–231.
19. Hore P. Solvent suppression in Fourier transform nuclear magnetic resonance. J Magn Reson 1983;55:283–300.

20. Pracht ED, Brenner D, Roebroeck A, Stöcker T. Ultra-high field optimization of the double inversion recovery (DIR) sequence: gray matter imaging at 7T. In Proceedings of the 22nd Annual Meeting of ISMRM, Milan, Italy, 2014. Abstract 0996.
21. Tesiram YA. Implementation equations for HSn RF pulses. J Magn Reson 2010;204:333–339.
22. Hennig J. Multiecho imaging sequences with low refocusing flip angles. J Magn Reson 1988;78:397–407.
23. Alsop DC. The sensitivity of low flip angle RARE imaging. Magn Reson Med 1997;176–184.
24. Stöcker T, Kaffanke J, Shah NJ. Whole-brain single-shot STEAM DTI at 4 Tesla utilizing transverse coherences for enhanced SNR. Magn Reson Med 2009;61:372–380.
25. Mugler JP, Epstein FH, Brookeman JR. Shaping the Signal response during the approach to steady state in three dimensional magnetization prepared rapid gradient echo imaging using variable flip angles. Magn Reson Med 1992;28:165–185.
26. Weigel M, Hennig J. Contrast behavior and relaxation effects of conventional and hyperecho-turbo spin echo sequences at 1.5 and 3 T. Magn Reson Med 2006;55:826–835.
27. Tannus A, Garwood M. Adiabatic pulses. NMR Biomed 1996;10: 423–434.
28. Brenner D, Tse DHY, Pracht ED, Feiweier T, Stirnberg R, Stöcker T. 3DREAM – a three-dimensional variant of the DREAM sequence In Proceedings of the 22nd Annual Meeting of ISMRM, Milan, Italy, 2014. Abstract 1455.
29. Nehrke K, Börnert P. DREAM-a novel approach for robust, ultrafast, multislice B1 mapping. Magn Reson Med 2012;68:1517–1526.
30. Bernstein MA, Fain SB, Riederer SJ. Effect of windowing and zero-filled reconstruction of MRI data on spatial resolution and acquisition strategy. J Magn Reson Imaging 2001;14:270–280.
31. Rooney WD, Johnson G, Li X, Cohen ER, Kim S-G, Ugurbil K, Springer CS. Magnetic field and tissue dependencies of human brain longitudinal 1H2O relaxation in vivo. Magn Reson Med 2007;57:308–318.
32. Yacoub E, Duong TQ, Van De Moortele P-F, Lindquist M, Adriany G, Kim S-G, Ugurbil K, Hu X. Spin-Echo fMRI in humans using high spatial resolutions and high magnetic fields. Magn 2003;49:655–664.
33. Wansapura JP, Holland SK, Dunn RS, Ball WS. NMR relaxation times in the human brain at 3.0 Tesla. J Magn Reson Imaging 1999;9: 531–538.
34. Robson PM, Grant AK, Madhuranthakam AJ, Lattanzi R, Sodickson DK, McKenzie CA. Comprehensive quantification of signal-to-noise ratio and g-factor for image-based and k-space-based parallel imaging reconstructions. Magn Reson Med 2008;60:895–907.
35. Norris DG, Lüdemann H, Leibfritz D. An analysis of the effects of short T2 values on the hyperbolic-secant pulse. J Magn Reson 1991; 92:94–101.
36. Gelderen P, van Jiang X, Duyn JH. Effects of magnetization transfer on T1 contrast in human brain white matter. Neuroimage 2016;128:85–95.
37. Eggenschwiler F, O'Brien KR, Gruetter R, Marques JP. Improving T2 -weighted imaging at high field through the use of kT-points. Magn Reson Med 2014;71:1478–1488.
38. Malik SJ, Padormo F, Price AN, Hajnal JV. Spatially resolved extended phase graphs: modeling and design of multipulse sequences with parallel transmission. Magn Reson Med 2012;68:1481–1494.
39. Lustig M, Donoho D, Pauly JM. Sparse MRI: the application of compressed sensing for rapid MR imaging. Magn Reson Med 2007;58: 1182–1195.
40. Gho S-M, Nam Y, Zho S-Y, Kim EY, Kim D-H. Three dimension double inversion recovery gray matter imaging using compressed sensing. Magn Reson Imaging 2010;28:1395–1402.